PERGAMON

Biomass and Bioenergy 23 (2002) 291–306

BIOMASS & BIOENERGY

www.elsevier.com/locate/biombioe

# Measurements and particle resolved modelling of heat-up and drying of a packed bed

Bernhard Peters[a,*], Elisabeth Schröder[a], Christian Bruch[b], Thomas Nussbaumer[c]

[a] *Research Centre Karlsruhe, Institute of Nuclear and Energy Technology, P.O. Box 3640, D-76021 Karlsruhe, Germany*
[b] *Eidgenössische Technische Hochschule Zürich, ETH Zentrum, CH-8092 Zürich Switzerland*
[c] *Verenum Research, Langmauerstr. 109, CH-8006 Zürich, Switzerland*

Received 15 May 2001; received in revised form 12 March 2002; accepted 12 March 2002

**Abstract**

The objective of this study is to measure the heat-up and the drying of a packed bed consisting of large wood particles as encountered in furnaces and to compare the predictions of a particle resolved approach to measurements. Within the experiments both single particle and packed bed measurements for the drying of wood were carried out. For both cases the samples as single particles and as a packed bed were exposed to a gas stream its temperature ranging from $T = 443$ to 743 K. The temperatures and the mass loss due to drying were recorded during the experiments and the heat transfer properties were correlated with earlier findings.

Within the present contribution a packed bed is considered as an ensemble of a finite number of particles. The heat-up and drying process of each particle is described by one-dimensional and transient conservation equations for mass and energy. Applying this model to all particles of a packed bed forms the entire packed bed process as a sum of individual particle processes. The arrangement of particles within the bed defines a solid phase and a void space between the particles. The flow through the void space of a packed bed is modelled as a flow through a porous media taking into account interaction between the solid and the gaseous phase by heat and mass transfer. A comparison between measurements and predictions of drying models yielded satisfactory agreement only for the constant evaporation temperature model. Furthermore, the results show, that a particle resolved approach is better suited than a continuum mechanic approach to describe packed bed processes since this approach omits additional empirical correlations for a packed bed. © 2002 Published by Elsevier Science Ltd.

*Keywords:* Particulate material; Heat and mass transfer; Packed bed; Drying; Numerical models

## 1. Introduction

Chemical processes involving a particulate phase are frequently encountered in technical applications, such as drying, reforming or catalytic regeneration in energy generation and processing industry. Therefore, research into a comprehensive model of a chemically reacting packed bed will be beneficial since basic understanding of the various processes taking place is fundamental to plant design, operation, and innovation. Experimental investigations into packed bed processes [1–4] usually are difficult to carry out due to a limited access inside the packed bed and therefore, demand a cost-intensive set-up. Numerical models [5] occur as a complimentary method to gain deeper knowledge of the processes in a packed bed.

Adams [6] developed a model consisting of layers for drying, pyrolysis and gasification of a packed

* Corresponding author. Tel.: +49-7247-823491; fax: +49-7247-824837.
*E-mail address:* b.peters@iket.fzk.de (B. Peters).

0961-9534/02/$ - see front matter © 2002 Published by Elsevier Science Ltd.
PII: S0961-9534(02)00052-1

**Nomenclature**

| | |
|---|---|
| $A$ | pre-exponential factor, depending |
| $c$ | concentration, kmol/m$^3$ |
| $c_p$ | constant-pressure specific heat, W/kg K |
| $c_v$ | constant-volume specific heat, W/kg K |
| $C$ | Forchheimer constant, 1/m |
| $d$ | diameter, m |
| $D$ | diffusion coefficient, m$^2$/s |
| $e$ | internal energy, J |
| $E_a$ | activation energy, J/mol |
| $f$ | correlation coefficient, dimensionless |
| $H_{evap.}$ | evaporation enthalpy, kJ/kg |
| $k$ | permeability, m$^2$ |
| $K$ | Forchheimer constant, m$^2$ |
| $P$ | porosity, dimensionless |
| $p$ | pressure, N/m$^2$ |
| $q$ | specific heat flux, W/m$^3$ |
| $r$ | independent variable, m |
| $m$ | mass, kg |
| $R_g$ | gas constant, J/mol K |
| $S$ | source term, depending |
| $S_i$ | inner surface, m$^2$ |
| $t$ | time, s |
| $T$ | temperature, K |
| $\vec{v}$ | velocity, m/s |
| $V$ | volume, m$^3$ |
| $Y$ | mass fraction, dimensionless |

*Greek letters*

| | |
|---|---|
| $\alpha$ | heat transfer coefficient, W/K m$^2$ |
| $\beta$ | mass transfer coefficient, m/s |
| $\gamma$ | contact angle, deg |
| $\Gamma$ | heat loss/gain, W/m$^3$ s |
| $\Delta$ | difference, dimensionless |
| $\varepsilon$ | porosity, dimensionless |
| $\eta$ | effectiveness factor, dimensionless |
| $\lambda$ | heat conductivity, W/m$^2$ K |
| $\mu$ | dynamic viscosity, kg/m s |
| $\rho$ | density, kg/m$^3$ |
| $\tau$ | tortuosity, dimensionless |
| $\omega$ | source term, depending |

*Subscripts*

| | |
|---|---|
| B | packed bed |
| cond | conduction |
| eff | effective values |
| g | gaseous phase |
| $i, j$ | specie |
| P | particle |
| rad | radiation |
| s | solid phase |
| $\infty$ | ambient value |

*Superscripts*

| | |
|---|---|
| $n$ | geometry exponent |

bed of wood. Each layer was described by conservation equations for mass and energy, whereby a chemical equilibrium determined the composition of the gasification layer. To describe the drying process of a packed bed, Raupenstrauch [7] supplied the two-dimensional Phoenics code, solving the conservation equations for the gaseous and the solid phase, with material properties and source terms. The solid phase is considered as a porous continuum with no detailed particle size distribution. The drying process is approximated by a heterogeneous reaction, for which the rate constants include effects of pure diffusion and heat–mass transfer [8]. Based on a one-dimensional homogeneous model Fatehi and Kaviany [9] predicted the propagation velocity of a conversion front through a fixed bed of wood dependent on the primary air-mass flux. A similar approach was carried out by Hartner [10], who described a reacting fixed bed by a one-dimensional and transient conservation equation for the gaseous and the solid phase. Beckmann and Scholz [11,12] approached the incineration of waste material on a travelling grate by cascade of well-stirred reactors. The thermodynamic and chemical state of each reactor is predicted by a global mass and energy balance. Therefore, each reactor requires empirical correlations, which are determined through experiments. Wakao et al. [13] presented two models to describe heat transfer in packed beds.

The continuous solid phase model (C-S-model) assumes the solid to be a continuous phase with heat conduction. Furthermore, thermal conversion of the fluid is taken into account also. The second model, labelled dispersion concentric model (D-C-model) is based on the fluid having a dispersed plug flow and the particle temperature field having radial symmetry. It is determined by the Laplace equation for intra-particle transport of heat. Describing all particles by such a rather uniform behaviour across the packed bed diminishes the effect of individual particle characteristics to some extent. However, Peters [14] extended this concept significantly by taking into account particles of different sizes, shapes and material properties. Moreover, simultaneous species and temperature distributions with sources for heat and mass are accounted for. Thus, he is able to resolve the thermal conversion behaviour of individual particles and its effect on the fluid flow through heat and mass transfer. This approach was applied partly by Bryden and Ragland [15] to simulate the incineration of entire tree trunks on a grate. They approximated the process by a conversion layer propagating through a trunk. The rate of drying, pyrolysis and combustion is derived by empirical correlation, which yielded a good agreement for the wood consumption rate with experiments. Skreiberg [16] developed a simulation method based on a global mass and energy balance to investigate the influence of parameters on a closed loop control during the incineration of a packed bed of wood. A similar model was developed by Kessel et al. [17] to predict the dynamical behaviour of waste incineration on a grate. In order to support the design of wood incineration plants, Kuo et al. [18,19] developed a one-dimensional model in conjunction with a global energy balance to predict conversion rate, thermal load of a grate and the gas phase. The approach, however, requires experimental correlations to describe major characteristics of the process. Krüll et al. [20] described the packed bed as a continuous porous media whereby the bed is divided into two layers with mass and energy balances for the solid and the gaseous phase. Their effort aimed to determine the release of species and energy from the packed bed to be coupled to a CFD-code as boundary conditions for the gas plenum above the packed bed. This was also carried out by Klasen and Görner [21] who determined the composition of the gas phase above the packed bed consisting of carbon-monoxide, carbon-dioxide and hydrocarbons dependent on the CH-ratio of the fuel. Likewise Riccius [22] incorporated an integral model into a CFD-code by determining a release of a representative hydrocarbon into the gas phase. Goh et al. [23] divided the packed bed above the grate into four layers representing fuel, drying, pyrolysis and ash. Each layer is described by integral balance equations, whereby the transport of energy only occurred normal to the grate through convection and an effective conductivity. Empirical correlations are required to describe the thermal conversion process adequately, which have to be determined experimentally for each fuel. Shin and Choi [24] developed a one-dimensional model to describe the incineration of wood for a laboratory scale furnace. Properties, originating from the wood particles, were lumped into integral values. Thus, the bed consists of moisture, char, volatiles and ash. The mass and heat transfer was determined by Nusselt and Sherwood numbers derived for packed beds taking the relevant surface area as the sum of particle surfaces. They use macro-kinetic data to characterise the conversion process dependent on the primary air supply and the calorific value of wood.

Common to the above-mentioned approaches, except the method of Bryden et al. [15] and Wakao [13], is, that a mainly one-dimensional treatment of a packed bed as a continuous two-phase system represents a rough approximation to the conversion processes and consequently, information originating from individual particle processes disappears by this approach. Therefore, these integral methods cannot predict the thermal conversion process sufficiently accurate and requires several empirical correlations to compensate for this loss of information.

However, this contribution deals with the development of a model to resolve the conversion process of a packed bed by describing the individual particle process with sufficient accuracy. Therefore, a single-particle model is developed, which can be applied to each particle of a packed bed and hence, represents the entire conversion of a packed bed as a sum of single-particle processes. The single-particle model is based on a system of one-dimensional transient conservation equations for mass and energy to predict major properties such as temperature and species distribution inside a particle. The particles are coupled to the surrounding gaseous phase by heat and mass

transfer. Furthermore, a description by conservation equations implies no restrictions on transport and kinetic time scales, so that it covers the entire range between the shrinking or the reacting core mode. The relevant information such as material properties and kinetic data is stored in a database, which allows an entire particle process to be represented through a combination of different processes. Hence, a wide range of applications is covered, which is easily extendable.

Due to the application to each particle of a packed bed, the complexity of the particle model is limited. Thus, effects like fragmentation, swelling or the detailed description of the boundary layer surrounding a particle are not included.

## 2. Experimental set-up

### 2.1. Introduction

The experiments investigating into the drying process of both a single-particle and a packed bed were set up to validate the present model approach based on a particle resolving level for a packed bed. Therefore, drying experiments were carried out in order to compare the predictions of heating-up and drying of large wood particles to measurements. Hereafter the successfully validated single-particle model was applied to each particle in a packed bed, so that the sum of all particle processes represents the entire packed bed process. The latter assumption, therefore, was validated by measurements of a packed bed.

### 2.2. Single-particle test facility

For the investigations into the drying of spherical wood particles under defined heat transfer conditions an experimental set-up as shown in Fig. 1 was used [25].

The drying chamber consists of a cylinder ($d = 5$ cm, $h = 10$ cm), which is insulated and electrically heated to the desired temperature. The wooden sample is suspended from scales to record the weight loss due to drying. Weight measurements are accurate within $\pm 5.75\%$. While the reactor heats up the sample is isolated from the chamber in order to avoid uncontrolled reactions during the heat-up period. At the start of the experiment, the sample is moved up into the drying chamber. A volumetric flux of $\dot{V}_{N_2} = 2$ l/s with a temperature of $T = 150^{\circ}$C was applied. The samples consisted of spherical beech wood particles ($d_p = 8$ mm) with an initial humidity of 67% as delivered from the forest. A different value of initial moisture ($x = 33\%$) to represent air-dry wood was achieved by a controlled pre-drying process.

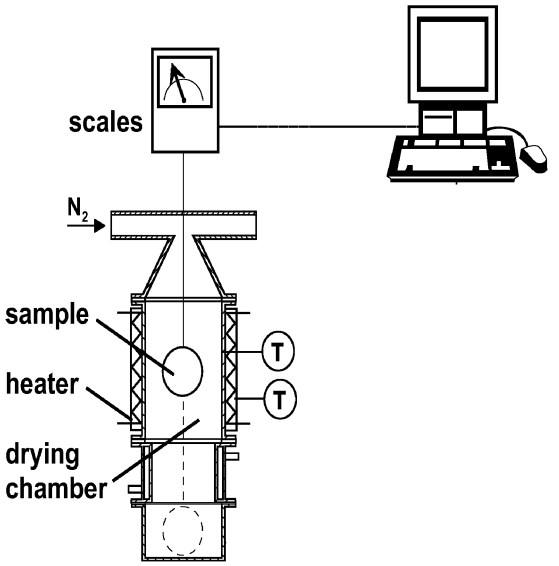


Fig. 1. Test facility for single-particle experiments.

### 2.3. Packed bed test facility

The test plant was designed to study the heating and the mass loss of a fixed bed of solid particles under conditions, encountered in municipal waste incinerators. The mass loss occurs when water contained in the bed evaporates. The experimental reactor shown in Fig. 2 consists of an outer steel cylinder designed for a maximum temperature of $T = 800^{\circ}$C and a maximum pressure of $p = 2$ bar.

The containment is electrically heated and thermally insulated at its cylindrical wall and the bottom to compensate heat losses. This assures no radial gradients of the temperature inside the packed bed. The top of the reactor is insulated, but not heated. The packed bed is filled into a cylindrical basket, which is positioned in the interior of the reactor. The fuel bed is 250 mm in diameter and 190 mm in height. Depending on the

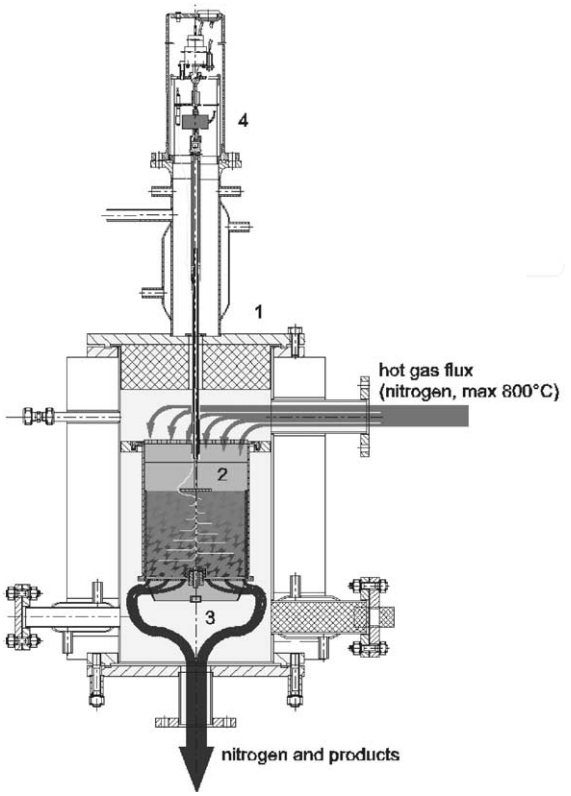


Fig. 2. Laboratory reactor PANTHA.

density of the packed bed material, its weight amounts to approximately 3 kg. A rod connects the basket containing the packed bed to a load cell. The load cell is located in a cold instrumentation compartment at top of the containment.

While the fuel bed is heated, the reaction chamber rests on an metal seat. In order to record mass losses due to evaporation and pyrolysis, the gas flow is turned off and the reaction tube is lifted via an electrical motor, which is connected with the load cell. The mass of the reaction tube, containing the solid particles, is detected for about 3 min. Afterwards the reaction tube is reinstalled in its previous position and the gas flow is turned on again. By adjusting the intervals of the weight measurements appropriately, a mass loss history for the packed bed due to evaporation is produced.

10 k-type thermocouples are positioned in the centre of the packed bed over its height to measure the temperature distributions and its dynamic behaviour

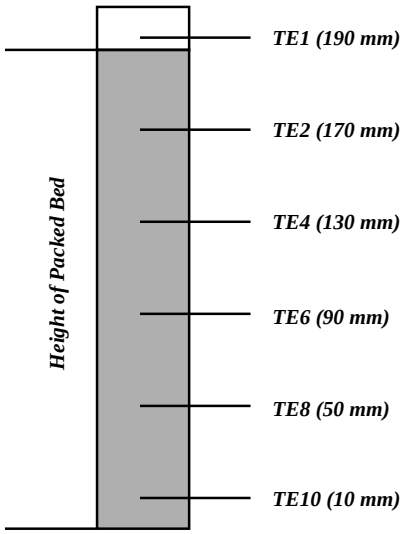


Fig. 3. Positions of thermocouples.

during heat-up and drying. The positions of the thermocouples is shown in Fig. 3.

Within the packed bed the thermocouples are spaced uniformly and one temperature is taken shortly above the surface of the packed bed to record the gas temperature of the hot air entering the bed at the top. It is covered with a porous plate to provide a plug flow profile for the incoming gas flow. Hence, the heating rate of the packed bed is adjusted by both the gas inlet temperature and the total flow rate. In order to reduce radial temperature gradients, the reactor is heated at its circumferential area in a closed loop mode.

The drying experiments were carried out with 2 kg of air-dried cubes 10 mm × 10 mm × 10 mm in size of beech wood. The moisture content of the particles is approx. 10% by mass. When the reaction tube has been filled with the particles, the steel containment is closed and preheated to approx. $T = 150^{\circ}$C by the circumferential electric heater. When the bed temperature rises to approx. $T = 90^{\circ}$C as a result of pre-heating, the hot gas flow is turned on. This moment is set as the beginning of the experiment.

Under the influence of the hot gas flow the temperature of the bed rises from top to bottom. The gas flow is turned off several times and the reaction tube is lifted to record the mass of the bed. Then the reaction tube is reinstalled and the gas flow is turned on again. The bed is heated to $T = 120^{\circ}$C, 135°C, and 150°C

When the desired bed temperature in the upper bed layers is reached, the gas temperature is kept constant. After approximately 10 000–12 000 s the bed temperature is isothermal and no further loss of mass can be achieved. Then the gas flow is stopped and the electric heaters are turned off. After the reactor has cooled down, the particles are taken out and weighed to close the mass balance.

The hot gas flow transports the moisture out of the reactor into the gas cooler where both the moisture and the gas are cooled to approx. $T = 20^{\circ}\mathrm{C}$. The moisture condenses, and the liquids are collected and weighed at the end of the experiment. There is a loss in the mass balance between the initial moisture and the water collected in the gas cooler because a certain amount of moisture remains gaseous and is carried out of the plant by the gas flow. When particles with low moisture content, such as beech wood, are used all moisture remains gaseous and no liquid can be found in the cooler. The mass loss history and the temperature profile of the experiments are compared with the numerical model of tools of object-oriented software for continuum-mechanics applications (TOSCA) [26,27].

## 3. Description of the models

### 3.1. Single-particle model

Since heat-up and drying depend strongly on temperature and water distributions in space and time, a model is required to resolve these characteristics in order to cover the range between transport and kinetically limited regimes. A separate description of heat/mass transfer and drying as chemical reaction eliminates the need for macro-kinetic data and promotes the use of data obtained under a solely kinetically controlled regime. Thus, limitation by transport or kinetics as is part of the integral models, e.g. reacting or shrinking core mode, is recognised by the model.

Although particulate material appears in a variety of different shapes it influences the chemical process only to a small extent as shown in Fig. 4 [28,29].

The Thiele-module expresses a ratio between a chemical and a diffusion time scale, whereas the effectiveness factor represents the ratio between the reactions taking place on the inner particle surface and the outer surface. The dimensionless numbers are defined as:

$$Th = \frac{AS_i r^2}{D}, \tag{1}$$

$$\eta = \frac{1}{3\Lambda^2}(3\Lambda \coth 3\Lambda - 1) \tag{2}$$

with $\Lambda$ as the square root of the Thiele module and $k, S_i, r$ and $D$ denoting the Arrhenius coefficient, inner surface, radius and diffusion coefficient. Although the lines for flat, long cylindrical and spherical particles cover a wide range of volume-to-surface ratios the difference in effectiveness factors turns out to be moderate, thus justifying the assumption that a spherical geometry can represent reasonably well various shapes. Further, evidence for this behaviour is provided by the experimental investigations of Senf [30]. His results indicate that the particulate matter (PM) emissions and volume-to-surface ratios are not correlated.

An unsteady and one-dimensional method for spherical particles combines a sufficient resolution of the particle quantities with reasonable computation time. The assumption of a one-dimensional behaviour is also supported by Man [31] who detected mainly one-dimensional behaviour in a comparison of his results with experimental data. Furthermore, a three-dimensional approach for a single particle

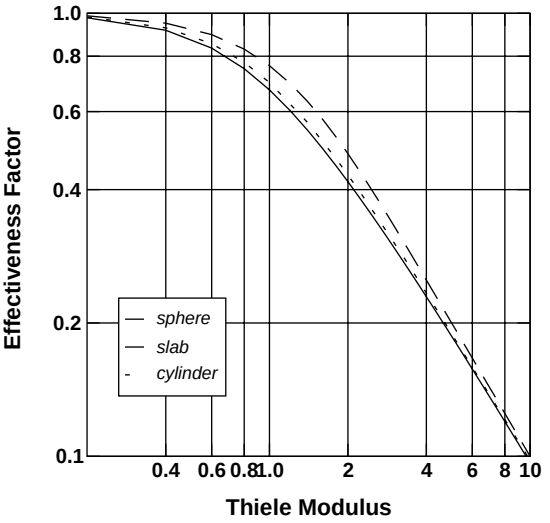


Fig. 4. Effectiveness of particle pores.

multiplied by its number in a packed bed would exceed computer resources currently available.

The volume-averaged quantities $\langle \Phi \rangle$ are derived from the phase-averaged $\langle \Phi \rangle^i$ quantities with the local value of the porosity. The conservation of a component $c_i$ in the porous gas phase depends on a chemical source term, a diffusive and a convective flux

$$\frac{\partial \langle c_{H_2O} \rangle}{\partial t} = \frac{1}{r^n} \frac{\partial}{\partial r} (D_{H_2O} r^n \frac{\langle c_{H_2O} \rangle^i}{\partial r} - r^n \langle \vec{v} c_{H_2O} \rangle) + \dot{\omega}_{c_{H_2O}}. \quad (3)$$

Due to the general formulation of the conservation equation the geometrical domain can be considered as an infinite plate ($n = 0$), an infinite cylinder ($n = 1$) or a sphere ($n = 2$).

Chan et al. [32] and Krieger-Brockett et al. [33] treat the drying process as a heterogeneous reaction according to

$$\dot{\omega}_{c_{H_2O}} = A e^{-E_a/RT} c_{H_2O} \quad (4)$$

for free and bounded water with its kinetic parameters $A = 5.13 \times 10^6$ 1/s, $E_{a,1} = 24$ kJ/mol and $E_{a,2} = 120$ kJ/mol. Evaporation of free and bound water employ an evaporation enthalpy of $H_{evap} = -48.6$ kJ/mol. $T$ and $c_{H_2O}$ are the temperature and concentration of water, respectively. This approach has the advantage of an activation energy accounting for both a temperature-dependent evaporation [7] and a varying strength of bound water and of being numerically stable. However, in this approach water already evaporates below the evaporation temperature. Moreover, it is difficult to apply the given kinetics to conditions different to these under which the data has been derived. This disadvantage can be compensated for by a method based on a thermodynamic balance between the energy available for evaporation and the amount of water evaporated [34,7]. It corresponds to the amount of heat above the evaporation temperature. Hence, any temperature increase above the evaporation temperature is consumed by the evaporation process. Since such a model includes a Dirac function, the equations become stiff and, therefore, appropriate solution techniques have to be employed.

For the constant evaporation model, the source term is defined as follows:

$$\dot{\omega}_{c_{H_2O}} = \begin{cases} \dfrac{(T - T_{evap.})\rho c_p}{H_{evap.} \delta t} & \text{if } T \geqslant T_{evap.}, \\ 0 & \text{if } T < T_{evap.}. \end{cases} \quad (5)$$

For this approach, heat available above the evaporation temperature $T_{evap.}$ is consumed by evaporation without distinguishing between bound and free water. Here $\rho$, $c_p$ and $H_{evap.}$ are the density and thermal capacity of dry wood and its evaporation enthalpy.

A contribution of the Knudsen diffusion is neglected due to an approximate value of the pore diameter of 50.0 μm [35,36] and a pressure of approximately 1 bar. Thus, only molecular diffusion in the pores, which are assumed homogeneously distributed, is taken into account. As a result of the averaging process and the influence of the tortuosity $\tau$ on the diffusion, an effective diffusion coefficient is derived as [37]

$$D_{H_2O,eff} = D_{H_2O} \frac{\varepsilon_P}{\tau}, \quad (6)$$

where $\varepsilon_P$ is the porosity of the particle and the molecular diffusion coefficients $D_{H_2O}$ are taken from the equivalent ones of the appropriate specie in nitrogen [38,39].

For the convective transport immediate outflow of the vapour without re-condensation is assumed. Therefore, a representative velocity in Eq. (3) is estimated by converting the sum of all reaction rates in a volume element $V_i$ into an out-streaming flux at its boundary surface $A_i$ according to

$$\vec{v} = \frac{V_i \sum_k \dot{\omega}_{H_2O}}{A_i \langle \rho_G \rangle}. \quad (7)$$

The density $\langle \rho_G \rangle$ of the gas mixture is determined by the equation of state.

Assuming thermal equilibrium between the gas phase, solid material and water, the energy conservation equation is given by

$$\frac{\partial \langle \rho c_p T \rangle}{\partial t} = \frac{1}{r^n} \frac{\partial}{\partial r} \left( r^n \lambda \frac{\partial \langle T \rangle}{\partial r} - r^n \langle \rho_G \vec{v} c_{p,G} T \rangle \right) + \dot{\omega}_{c_{H_2O}} H_{evap.}. \quad (8)$$

The locally varying transport coefficient $\lambda_{eff}$ is approximated by the following expression [36]:

$$\lambda_{eff} = \varepsilon_P \lambda_g + \lambda_{wood} + \lambda_{rad} \quad (9)$$

which takes into account heat transfer by conduction in the gas, solid and radiation in the pore. The latter is believed to be significant at higher temperatures [40]. The convective term as a further mechanism of transport is estimated by the velocity of Eq. (7). The source term stands for heat consumed by evaporation weighted by the respective enthalpy.

For mass and heat transfer of a particle, the following boundary conditions are applied:

$$-D_{\mathrm{H_2O,eff}}\frac{\partial\langle c_{\mathrm{H_2O}}\rangle}{\partial r}|_R = \beta_{\mathrm{H_2O}}(\langle c_{\mathrm{H_2O},R}\rangle - c_\infty), \tag{10}$$

$$-\lambda_{\mathrm{eff}}\frac{\partial\langle T\rangle}{\partial r}|_R = \alpha(\langle T_R\rangle - T_\infty) + \dot{q}_{\mathrm{cond}} \tag{11}$$

where $c_{i,\infty}$, $T_\infty$, $\beta$ and $\alpha$ stand for the ambient gas concentration, temperature, mass and heat transfer coefficients, respectively. Additionally to the convective heat transfer, a conductive flux $\dot{q}_{\mathrm{cond}}$ between particles in contact can be taken into account. The conductive heat flux between two neighbouring particles in contact is estimated by

$$\dot{q}_{\mathrm{cond}} = -\frac{1}{1/\lambda_1 + 1/\lambda_2}\frac{\partial T}{\partial r} = -\frac{1}{1/\lambda_1 + 1/\lambda_2}\frac{T_{S,1} - T_{S,2}}{\Delta r_{S,1} - \Delta r_{S,2}}, \tag{12}$$

where the temperature gradient between two particles is approximated by the temperature difference between the outer shell values of the particles and its distance $\Delta r_{S,i}$ to the outer particle surface. The conductivities $\lambda_1$ and $\lambda_2$ refer to the particles in contact, respectively. The contact area is assumed quadratic and is determined by the contact angles $\gamma_1$ and $\gamma_2$ by $A_c = 1/2\ ((R_1 \tan\gamma_1)^2 + (R_2 \tan\gamma_2)^2)$ as sketched in Fig. 5.

Due to the efflux of volatiles and steam from the particle the Stefan correction is introduced into the transfer coefficients, which are estimated as follows:

$$\beta = \frac{\dot{m}_g/\rho_g}{\exp(\dot{m}_g/\rho_g\beta_0) - 1}, \tag{13}$$

$$\alpha = \frac{\dot{m}_g c_{p,g}}{\exp(\dot{m}_g c_{p,g}/\alpha_0) - 1}, \tag{14}$$

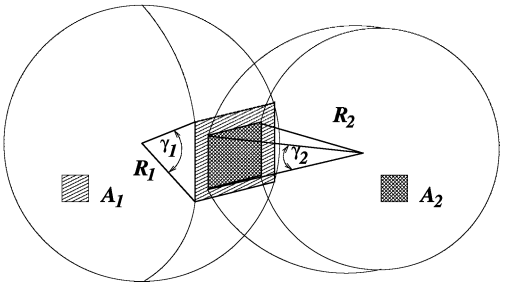


Fig. 5. Conduction between two neighbouring particles.

where $\alpha_0$ and $\beta_0$ denote the transfer coefficients for a vanishing convective flux over the particle surface. In a packed bed the mass and heat transfer rates, respectively, the Nusselt and Sherwood numbers are augmented by the tortuosity of the flow paths as compared to a single particle [41]. According to Schlünder et al. [42] the appropriate Nusselt number $Nu_B$ and Sherwood number $Sh_B$ for a packed bed are derived from the one of a single particle by $Nu_B = f\ Nu_S$ and $Sh_B = f\ Sh_S$. The correlation coefficient $f$ is determined by the following relationship [43] $f = 1 + 1.5(1 - \varepsilon_P)$ with $\varepsilon_P$ denoting the void fraction of the packed bed. Thus, mass and heat is transferred into the gaseous flow in the void space of a packed bed, where the transferred quantities appear as source terms in the appropriate conservation equations, as described in the following chapter.

### 3.2. Bed model

If a small fraction is extracted from a packed bed it may have the appearance shown in Fig. 6 [44].

Part of the element is made up of solid material, whereas the remaining void space is occupied by the gas phase. Between the solid phase and the gas phase various mass and heat transfer mechanisms take place which are caused by evaporation. The gas flow in the void space between the particles of the bed is treated as a flow through porous media according to Darcy's law.

The gas flow in a porous medium is compressible, and various transient effects make it an unsteady motion. The momentum due to mass transfer from particle surfaces into the gas phase is negligible. Because of the existence of different components in the flow

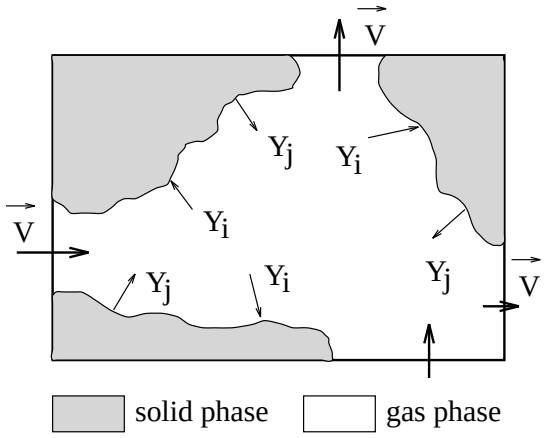


Fig. 6. Extraction of a packed bed.

the gas phase is treated as a perfect mixture of perfect gaseous components to which the equation of state applies.

Under the assumptions outlined above the resulting set of coupled non-linear differential equations for mass, momentum, energy and species together with the equation of state are summarised below in vector form and in Cartesian coordinates.

*Continuity*:

$$\frac{\partial \rho_g}{\partial t} + \nabla \cdot (\rho_g \vec{v}_g) = S_g. \tag{15}$$

Here $\rho_g$ and $v_g$ are gas density and velocity at a position and time $t$, respectively. The source term on the right-hand side includes mass transfer rates between the solid and the gaseous phases due to evaporation of water inside the particle.

*Momentum*:

$$\frac{\partial(\rho_g \vec{v}_g)}{\partial t} + \nabla \cdot (\rho_g \vec{v}_g \vec{v}_g) = -\nabla p_g + F(\vec{v}_g), \tag{16}$$

where $p_g$ stands for the gas pressure.

The function $F(\vec{v}_g)$ accounts for different flow regimes defined by Eq. (17). For high particle densities as it is the case in the current study viscous shear stresses are negligible compared to the drag forces and have therefore been omitted in the momentum equation. Experimental measurements [45] have shown that Darcy's law is valid for a Reynolds number based on $\sqrt{k}$, with $k$ denoting the permeability, smaller than $\sim$ 10. Above this value inertia effects reminiscent of turbulent flow over a rough surface introduce a non-linear behaviour, which leads to Forchheimer's equation as a modification of Darcy's law.

$$F(\vec{v}_g) = \begin{cases} -\dfrac{\mu}{k}\vec{v}_g & \text{if } Re < 10, \\ -\dfrac{\mu}{K}\vec{v}_g - \rho_g C \vec{v}_g |\vec{v}_g| & \text{if } Re \geqslant 10, \end{cases} \tag{17}$$

where $k$ is the permeability and $K$ and $C$ are constants of the form [46,47]:

$$K = \frac{d^2 P^3}{150(1-P)^2}, \tag{18}$$

$$C = \frac{1.75(1-P)}{dP^3}. \tag{19}$$

*Vapour*:

$$\frac{\partial(\rho_g Y_{H_2O,g})}{\partial t} + \nabla \cdot (\rho_g \vec{v}_g Y_{H_2O,g}) = \nabla \cdot (D_{H_2O,g} \nabla Y_{H_2O,g}) + S_{Y_{H_2O,g}}, \tag{20}$$

where $Y_{H_2O,g}$ and $D_{H_2O,g}$ are the vapour mass fraction and its diffusion coefficient, respectively. The source term $S_{Y_{H_2O,g}}$ takes into account mass sources due to evaporation from a particle.

*Energy*:

$$\frac{\partial(\rho_g e_g)}{\partial t} + \nabla \cdot (\rho_g \vec{v}_g e_g) = \nabla \cdot (\lambda_g \nabla T_g) - \nabla \cdot p_g \vec{v}_g - F(\vec{v}_g)\vec{v}_g + \Gamma. \tag{21}$$

Here $\Gamma$ is the heat loss/gain of the gas at the walls.

$$e = c_{v,g} T_g \tag{22}$$

is the specific internal energy, given by the product of constant-volume specific heat $c_{v,g}$ weighted by mass fractions and gas temperature $T_g$.

Equation of state (for an assumed perfect gas):

$$\frac{p}{\rho} = RT, \tag{23}$$

where $R$ is the gas constant. The emissive and adsorptive properties of the gas phase are negligible because of short ray travelling distances and low concentration of vapour.

## 4. Results

Since in the present contribution a packed bed is regarded as an ensemble of particles model validations and predictions were carried out for both a single particle and a packed bed of particles. For the latter the single-particle model is applied to each particle including interaction with neighbouring particles and the surrounding flow field of a packed bed and thus, describing the entire heat-up and drying process of a packed bed. Furthermore, a particle resolved approach requires mainly validation of a single-particle model, which reduces experimental investigations compared to experiments for an entire packed bed significantly. The single particle model offers a high level of detailed information. Due to the model's level of resolution it is assumed to omit empirical correlations which makes it independent of particular experimental conditions.

### 4.1. Predictions for a single particle

After the heat-up process for the three different geometries, e.g. plate, cylinder and sphere were successfully compared to the analytical solution the drying processes of a spherical fir wood particle was predicted and compared to measurements. The relevant wood properties are listed in Table 1.

A wall temperature of $T_{heat} = 743$ K was set for the experiment while immediate outflow of vapour was assumed due to an increasing inner particle pressures. The process of drying was described by two approaches: one approximates the evaporation based on an energy balance (Eq. (5)) in conjunction with a given evaporation temperature, whereas the second approach represents a heterogeneous reaction between liquid water and vapour (Eq. (4)) [32,33].

Table 1
Properties of fir wood [35,36]

| | |
|---|---|
| Particle radius R | 4 mm |
| Density $\rho$ | 330 kg/m$^3$ |
| Porosity $\varepsilon_P$ | 0.6 |
| Pore diameter $d_p$ | $50.0 \times 10^{-6}$ m |
| Tortuosity $\tau$ | 1.0 |
| Diffusivity $D$ | $1.1 \times 10^{-4}$ m$^2$/s |
| Specific heat $c_p$ | 1733.0 J/kg K |
| Conductivity $\lambda_{wood}$ | 0.2 W/m K |

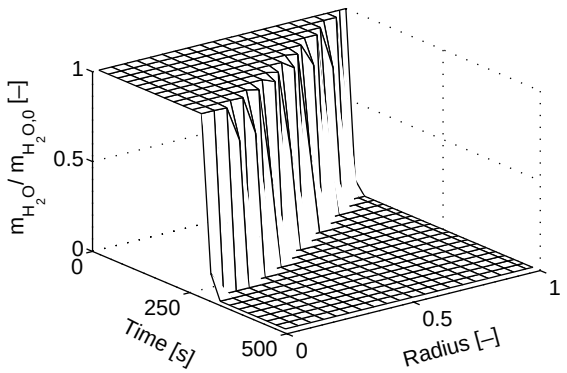


Fig. 7. Drying of a particle modelled by an energy balance.

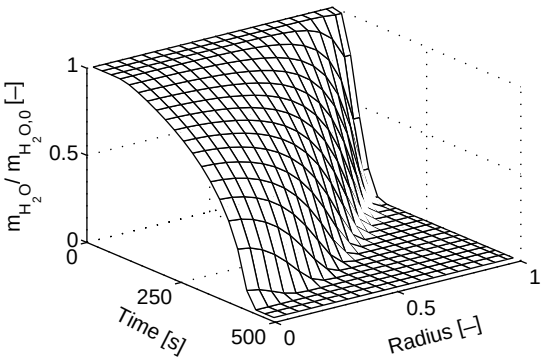


Fig. 8. Drying of a particle modelled by a heterogeneous reaction.

Figs. 7 and 8 depict the diminishing content of water versus time and dimensionless radius as predicted by the two models.

The prediction of the evaporation temperature model obviously result in steep gradients, which effectively represents a drying front propagating into the particle. This formulation strongly couples the drying process to the temperature and thus, to the transport of heat within a particle. The alternative model based on a heterogeneous reaction develops at the start of the drying process steep gradients as shown in Fig. 8. Then, while the drying process advances, gradients become smoother because no lower cut-off as an evaporation temperature exists. Compared to the previous predictions the drying rate is lower, which results in an extended drying period of approximately 150 s.

The corresponding temperature profile and its evolution in time is shown in Fig. 9.

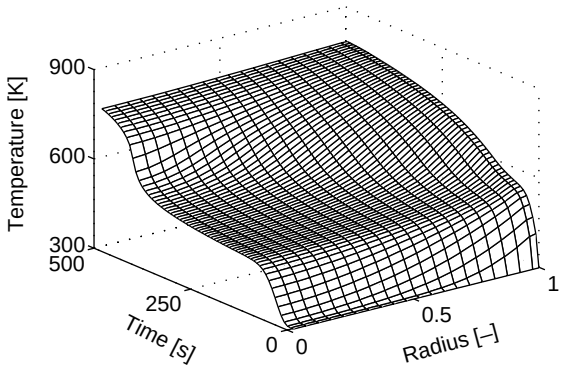


Fig. 9. Temperature during drying of a particle.

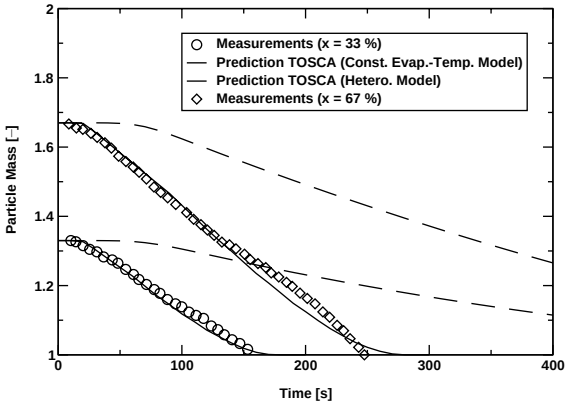


Fig. 10. Comparison between measurements and predictions.

After a short heat-up period with negligible evaporation, a plateau like distribution of a constant temperature dominates the dynamic behaviour. During this period, the temperature is high enough to provide a considerable evaporation rate, which consumes heat within the particle. Only, after the water content in a shell layer is entirely evaporated, temperature increases again to provide heat for the evaporation process of inner layers.

These results were related to experiments of spherical particles of wet fir wood with a moisture content of 33% and 67% and are shown in Fig. 10.

The constant evaporation temperature model agrees satisfactorily with both experiments. The heterogeneous reaction model, however, underpredicts the drying rate significantly and thus, leads to extended drying times. Therefore, this approach is not suited to the present application of large wood particles. It is assumed that the kinetic parameters of this model reflect partly experimental parameters such as heat transfer and therefore, cannot be employed under different conditions.

Table 2
Properties of aluminium and slate

| | Aluminium | Slate |
|---|---|---|
| Density $\rho$ | 2700 kg/m$^3$ | 1440 kg/m$^3$ |
| Specific heat $c_p$ | 896 J/kg K | 0.82 J/kg K |
| Conductivity $\lambda$ | 229 W/m K | 0.16 W/m K |
| Diameter $d$ | 7 mm | 12.6 mm |
| Void fraction $\varepsilon_B$ | 0.57 | 0.52 |
| References | [48] | [49,50] |

### 4.2. Predictions for a packed bed

In a first step the particle resolved approach was applied to predict heating of a packed bed and the results obtained were compared to measurements [1]. This represents solving the energy equation for each particle, taking into account conduction between particles and convective heat transfer between the particles and the surrounding flow field. Due to a low temperature range, radiation heat transfer is neglected. Both experiments and predictions were carried out for aluminium and slate as representatives of a high- and a low-conductive material. Their properties are listed in Table 2.

The flux of heated air amounted to $\dot{m} = 16$ kg/h with a temperature of $T_g = 300^\circ$C with the heat transfer conditions determined by Eq. (14). Fig. 12 depicts the profile of the incoming gas temperature and the transient distribution of temperatures along the height of a packed bed of aluminium spheres and slate as a representative of low conductivity. Due to a low-temperature range, radiation heat transfer is neglected.

Within initial experiments the heat transfer conditions inside the packed bed were investigated by Schröder [51]. By measuring the inner particle temperature and the temperature of the surrounding gas phase, the heat transfer coefficient was determined depending on the local flow conditions. The results were compared to various correlations from

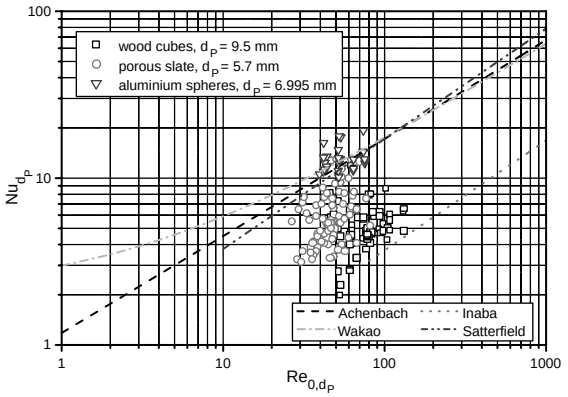


Fig. 11. Heat transfer conditions in a packed bed.

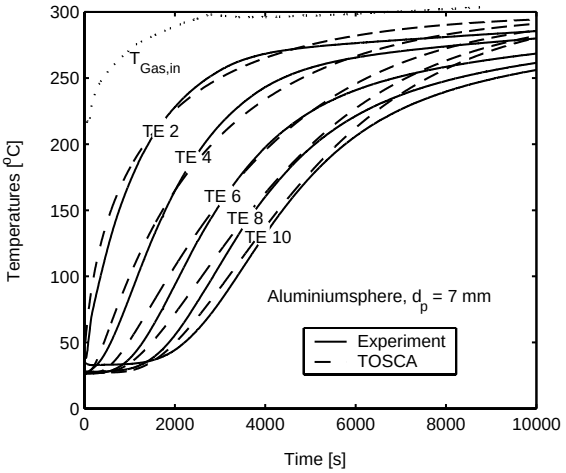


Fig. 12. Heat-up of a packed bed (Aluminium).

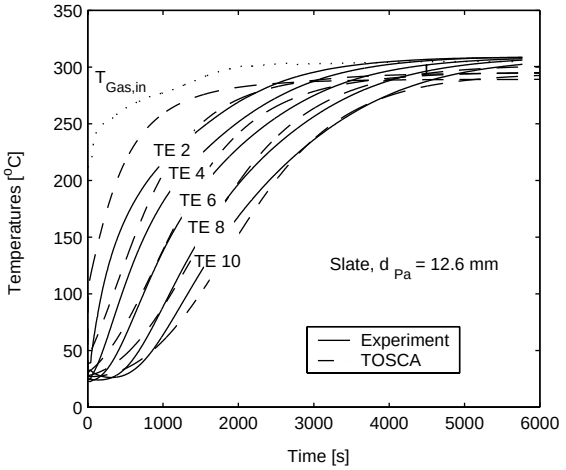


Fig. 13. Heat-up of a packed bed (slate).

literature [52,13,53,54] and are shown for wood, slate and aluminium in Fig. 11.

For the experiments with spherical aluminium particles a good agreement with the correlation of Achenbach [52], Wakao [13] and Satterfield et al. [54]. Nusselt numbers for wood and slate are estimated lower than predicted by the correlations, which Schröder attributes to inaccurate properties of these materials. The deviations between the empirical correlations in particular for Reynolds numbers $Re < 200$ is due to radial dispersion and non-uniform flow behaviour as pointed out by the respective authors. However, the comparison between experimental data and empirical correlations shows, that the latter may be applied with sufficient accuracy to packed beds to determine heat transfer between gas and solid phase.

Fig. 12 depicts the transient temperature profiles along the height of a packed bed of aluminium spheres ($d = 7$ mm).

The labels to the temperature profiles refer to the positions shown in Fig. 3. The comparison of the dynamical behaviour between measurements and predictions shows good agreement. Deviations occur for the steady-state values of the temperature, because the predictions were obtained under adiabatic conditions, whereas the experiments lacked of a perfect insulation.

Fig. 13 shows similar temperature profiles for the heat-up of a packed bed of slate material ($d = 12.6$ mm) as a representative of low conductivity.

Again, the predictions agreed satisfactorily with measurements considering the uncertainty of measuring either gas or particle temperatures in a packed bed.

Following this validation to predict the temperature evolution in a packed bed, its drying process for beech wood particles were calculated. The relevant properties of beech wood, taken from Kung [55], are listed in Table 3.

The following Figs. 14–16 depict the drying process as a mass loss history of beechwood particles with a moisture content of 10%.

The drying temperature of the incoming gas was adjusted at $T = 120^{\circ}$C, 135°C and 150°C, whereby the

Table 3
Beech wood properties

| | |
|---|---|
| Particle radius R (mm) | 6.2 |
| Density $\rho$ (kg/m$^3$) | 750 |
| Porosity $\varepsilon$ | 0.64 |
| Permeability $k$ | 0.02 |
| Pore diameter (m) | $50.0 \times 10.0^{-6}$ |
| Tortuosity | 1.0 |
| Specific heat $c_p$ (J/kg K) | 2551.3 |
| Conductivity $\lambda$ (W/m K) | 0.1256 |
| Void fraction $\varepsilon_B$ | 0.46 |

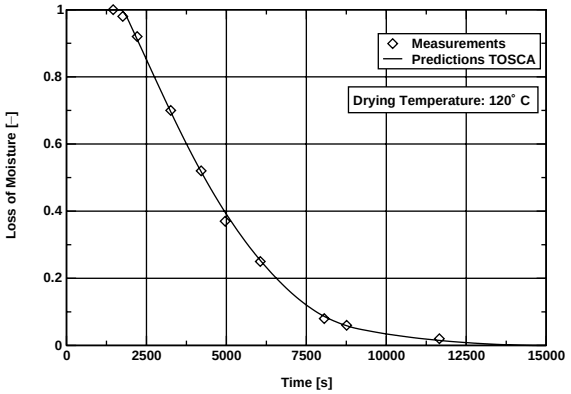


Fig. 14. Drying of a packed bed of beech wood.

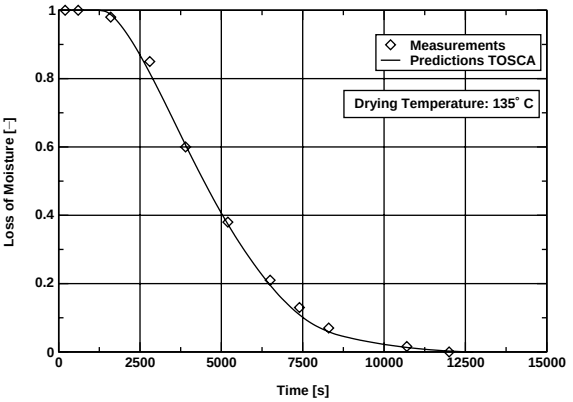


Fig. 15. Drying of a packed bed of beech wood.

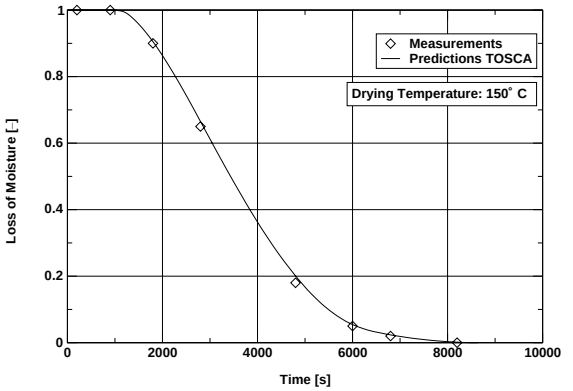


Fig. 16. Drying of a packed bed of beech wood.

upper temperature was chosen as to prevent thermal decomposition of the wood particles due to pyrolysis.

The comparison between measurements and predictions for each case shows good agreement, which proves that the evaporation temperature model without further empirical correlations neither for a single particle nor for the packed bed is suited as a drying model for large wood particles and that the novel approach with a particle resolving description of a packed bed performs well.

## 5. Conclusions

The novelty of the current contribution is to extend a particle-resolving approach for a packed bed to its thermal conversion processes such as heat-up and drying. Within the current study particles may have different sizes, shapes or properties. Heat-up and drying are calculated for each particle by transient and one-dimensional conservation equations for mass and energy. The sum of all particle processes represents the entire thermal conversion process of a packed bed. It includes interaction between the gaseous and the solid phase via heat and mass transfer. The suitability of the particle resolved approach is proven by well-predicted results in comparison with measurements for both a single particle and a packed bed under various boundary and initial conditions. Among the two models to describe a drying process, the evaporation temperature model has manifested its superiority over the heterogeneous reaction approach for large wood particles. These findings suggest, that for large wood particles and medium heat transfer rates as encountered under technically relevant conditions the evaporation process is limited by heat transfer. Since no further empirical correlations are required,

experimental investigations are reduced significantly. This is due to the fact that mainly only a single particle model has to be validated as compared to an entire packed bed model. Concluding the present findings encourage the application of this approach to pyrolysis and combustion of a packed bed.

## Appendix A. Discretisation procedure and solution algorithm

To the conservation equations of both the particle and the gas flow in the void space of the packed bed a time-marching finite-volume approach is employed to obtain the solution of the relevant variables [56]. Within the method the geometry is divided into non-overlapping control volumes. One of the most attractive features of this type of formulation is that it obeys integral conservation of quantities such as mass and energy at each cell and therefore, over the whole domain. An implicit and explicit scheme is implemented. However, due to a large variety of time scales, e.g. reaction and diffusion time scales inherent in the system the implicit approach is favoured as there is no limitation by the stability criteria of Courant for the smallest time scale. Each equation of the system may be represented by the following general formulation for the conservation of a scalar $\Phi$:

$$\frac{\partial}{\partial t}(\langle\rho\rangle\langle\Phi\rangle) = \frac{1}{r^n}\frac{\partial}{\partial r}\left[\Gamma r^n \frac{\partial\langle\Phi\rangle}{\partial r} - \rho_g r^n v_D\langle\Phi\rangle\right] + \dot{\omega}_\Phi. \tag{A.1}$$

Integrating Eq. (A.1) over a control volume with its volume $V$ and surface $A$ and applying Gauss' theorem gives

$$\int_V \frac{\partial}{\partial t}(\langle\rho\rangle\langle\Phi\rangle)\,\mathrm{d}V = \int_A [\Gamma\frac{\partial\langle\Phi\rangle}{\partial r} - \rho_g v_D\langle\Phi\rangle]\,\mathrm{d}A + \int_V \omega_\Phi\,\mathrm{d}V. \tag{A.2}$$

For sufficient small time steps the integrand is assumed constant, so that the evaluation of the volume integrals yields the volume and the boundary integrals can be approximated by a sum as follows:

$$\frac{\partial}{\partial t}(\langle\rho\rangle\langle\Phi\rangle)V = \sum_{A_i}\left[\Gamma\frac{\partial\langle\Phi\rangle}{\partial r} - \rho_g v_D\langle\Phi\rangle\right]A_i + \omega_\Phi V. \tag{A.3}$$

Introducing a spatial discretisation scheme into Eq. (A.3) reduces it to a system of coupled ordinary differential equations, which has the following general form:

$$\dot{y} = f(t, y), \quad y(t_0) = y_0 \tag{A.4}$$

where $\dot{y}$ denotes the derivative $\mathrm{d}y/\mathrm{d}t$. In order to solve the relevant variables a time integration has to be performed. For the gas flow in the void space an implicit Euler method is applied, whereas the same method for the time integration of the particle model is not sufficient due to the stiffness of the equations.

As the transient character of species and energy distributions varies to a large extent, at least one component of the solution decays much faster, i.e. the Jacobian matrix $J = \partial f/\partial y$ has an eigenwert with a large negative real part. This fact introduces a considerable stiffness into the system, which is typical for engineering applications. Conventional methods such as Euler, explicit Runge–Kutta and Adams–Moulton are restricted to a very small step size that the solution behaves stable. This means that considerable computer time would be required. Therefore, a multi-step method which is capable to handle the stiff systems of equations has to be chosen here. In particular a backward-differencing scheme of order 1–5 fulfils the requirements for the current application [57]. For the implementation of the solver the software library TOSCA [26] has been combined with the software package ODE++ [58,59], allowing easily to exchange the solver method if required. The numerical solution to Eq. (A.4) is generated as discrete values $y_n$ at time points $t_n$. Here, the values $y_n$ obey a linear multi-step formula

$$y_n - \sum_{i=1}^{q}\alpha_{n,i}y_{n-i} - h_n\beta_{n,0}\dot{y}_n = 0, \tag{A.5}$$

where $\alpha_{n,i}$ are the weighting coefficients and the order $q$ varies between 1 and 5. The $\dot{y}_n$ are computed approximations to $\dot{y}(t_n)$ with a step-size $h_n = t_n - t_{n-1}$. The non-linear system of Eq. (A.5) for the calculation of a new $y_n$ is solved by a modified Newton method, in which a predictor is followed by successive correctors until the required error tolerance is satisfied.

## References


[1] Schröder E. Stand des Entwurfs der Pyrolyseanlage PANTHA. Technical report, Forschungszentrum Karlsruhe, 1996.

[2] Hellwig M. Zum Abbrand von Holzbrennstoffen unter besonderer Berücksichtigung der zeitlichen Abläufe. Ph.D. thesis, Technische Universität München, 1988.

[3] Zhou X. Contribution à l'étude de l'incinération des déchets urbains: expérimentation en réacteur à lit fixe à contre courant, approche théorique du déplacement du front d'inflammation. Ph.D. thesis, University of Poitiers, 1994.

[4] Rogers JEL, Sarofim AF, Howard JB, Wiiliams GC, Fine DH. Combustion characteristics of simulated and shredded refuse. Proceedings of the 15th Symposium (International) on Combustion, Vol. 15, 1975. p. 1137–48.

[5] Smoot LD. Fundamentals of coal combustion for clean and efficient use. Amsterdam: Elsevier, 1993.

[6] Adams T. A simple fuel bed model for predicting particulate emissions from a wood waste boiler. Combustion and Flame 1980;39:225–39.

[7] Raupenstrauch H. Ein Beitrag zur Computersimulation reagierender Schüttschichten. Ph.D. thesis, TU Graz, 1991.

[8] Chan W.-C.R, Kelbon M, Krieger B. Product formation in the pyrolysis of large wood particles. In: Overend RP, Milne TA, Mudge LK., editors. Fundamentals of thermo-chemical biomass conversion. Papers from the Int. Conf. in Estes Park, Colorado: Elsevier Applied Science Publisher, London, 1985. p. 219–36.

[9] Fatehi M, Kaviany M. Adiabatic reverse combustion in a packed bed. Combustion and Flame 1994;99:1–7.

[10] Hartner P. Entwicklung eines Computerprogramms zur eindimensionalen Simulation von heterogenen Festbett- und Vorschubreaktoren. Ph.D. thesis, Technische Universität Graz, 1996.

[11] Beckmann M, Scholz R. Zum Feststoffumsatz bei Rückständen in Rostsystemen. Brennstoff-Wärme-Kraft 1994;46(5):218–29.

[12] Beckmann M, Scholz R. Simplified mathematical model of combustion in stoker systems. Proceedings of the Third European Conference on Industrial Furnaces and Boilers, Porto, Portugal, 18–21 April 1995. S61–70.

[13] Wakao N, Kaguei S. Heat and mass transfer in packed beds. London: Gordon and Breach, 1982.

[14] Peters B. A detailed model for devolatilization and combustion of waste material in packed beds. Proceedings of the Third European Conference on Industrial Furnaces and Boilers. Porto, Portugal, 1995. p. S86–104.

[15] Bryden K, Ragland K. Numerical modeling of a deep, fixed bed combustor. Energy and Fuels 1996;10:269–75.

[16] Skreiberg ø. Woodsim—a mass and heat balance program for batch combustion processes of solid fuels. IEA Bioenergy Working Group Meeting, 6 June, Norway, 1997.

[17] van Kessel LBM, Brem G. A dynamic model of a municipal waste incinerator. VDI Bericht 1995;1193:421–8.

[18] Kuo JT, Hsu WS, Yo T-C. Effect of air distribution on solid fuel bed combustion. Journal of Energy Resources Technology 1998;119:120–8.

[19] Kuo JT. Estimation of burning rates in solid waste combustion furnaces. Combustion Science and Technology 1998;137: 1–29.

[20] Krüll F, Kremer H, Wirtz S. Feuerraumsimulation einer Müllverbrennungsanlage bei gleichzeitiger Simulation der Verbrennung auf dem Rost. VDI Bericht 1390, Modellierung und Simulation von Dampferzeugern und Feuerungen, 1998. p. S199–212.

[21] Klasen Th, Görner K. Simulation und Optimierung einer Müllverbrennungsanlage. VDI Bericht 1390, Modellierung und Simulation von Dampferzeugern und Feuerungen, 1998. p. S227–41.

[22] Riccius O. CFD-Einsatz für Müllverbrennungsanlagen. VDI Bericht 1390, Modellierung und Simulation von Dampferzeugern und Feuerungen, 1988. p. S215–26.

[23] Goh YR, Siddall RG, Nasserzadeh V, Zakaria R, Swithenbank J, Lawrence D, Garrod N, Jones B. Mathematical modelling of the burning bed of a waste incinerator. Journal of the Institute of Energy 1998;71:110–8.

[24] Shin DH, Choi S. The combustion of simulated waste particles in a fixed bed. Combustion and Flame 2000;121:167–80.

[25] Bruch Ch. Beitrag zur Modellierung der Festbettverbrennung in automatischen Holzfeuerungen. Ph.D. thesis, ETH Zürich, No. 14040, 2000.

[26] Peters B. Efficient software development and use for engineering applications with TOSCA (Tools of Object-Oriented Programming for Continuum Mechanic Applications). In: CFD 96, Fourth Annual Conference of the CFD Society of Canada, Ottawa, Ontario, Canada, June 1996. p. 2–4.

[27] Peters B. Application de la conception objet orienté à la modélisation de l'incinération de déchets municipaux. In: Informatique pour l'Environnement'97.

[28] Bird RB, Stewart WE, Lightfoot EN. Transport phenomena. New York: Wiley, 1960.

[29] Fromment GF, Bishhoff KB. Chemical reactor analyses and design. New York: Wiley, 1979.

[30] Senf N. Low emissions residential cordwood combustion in high mass appliances—recent research and results. In: Combustion Canada '96, Ottawa, Ontario, Canada, June 5–7, 1996.

[31] Man YH, Byeong RC. A numerical study on the combustion of a single carbon particle entrained in a steady flow. Combustion and Flame 1994;97:1–6.

[32] Chan WR, Kelbon M, Krieger BB. Modelling and experimental verification of physical and chemical processes during pyrolysis of a large biomass particle. Fuel 1985;64:1505–13.

[33] Krieger-Brockett B, Glaister DS. Wood devolatilization—sensitivity to feed properties and process variables. In: Bridgewater AV, editor. International Conference on Research in Thermochemical Biomass Conversion, 1988. p. S127–42.

[34] Cenkowski S, Jayan DS, Pabis S. Deep bed grain drying: a review of particular theories Drying Technology 1993;11(7):1553–81.

[35] Seebauer V, Petek J, Staudinger G. Effects of particle size, heating rate and pressure on measurement of pyrolysis

kinetics by thermogravimetric analysis. Fuel 1997;76: 1277–82.
[36] Grønli M. A theoretical and experimental study of the thermal degradation of biomass. Ph.D. thesis, NTNU Trondheim, 1996.
[37] Rummer B, Petek J, Staudinger G. Trocknung und Pyrolyse eines Einzelpartikels—Modellrechnung und experimentelle Verifikation. Dusseldorf: VDI Verlag, 1997.
[38] Shih-I Pai. Two-phase flows, Vieweg Tracts in Pure and Applied Physics. Braunschweig: Vieweg, 1977.
[39] Dullien FAL. Porous media fluid transport and pore structure. New York: Academic Press, 1979.
[40] Hottel HC, Sarofin AF. Radiative transfer. New York: McGraw-Hill Book Company, 1967.
[41] Baehr HD, Stephan K. Wärme- und Stoffübertragung. 1. Auflage. Berlin: Springer, 1994.
[42] Schlünder EU, Tsotsas E. Wärmeübertragung in Festbetten, durchmischten Schüttgütern und Wirbelschichten. Stuttgart: G. Thieme Verlag, 1988.
[43] Gnielinski V. Berechnung des Wärme- und Stoffaustauschs in durchströmten ruhenden Schüttungen. Verfahrenstechnik 1982;16:36–9.
[44] Peters B. Kfk 5385. Technical report, Nuclear Research Center Karlsruhe, 1994.
[45] Ward JC. Turbulent flow in porous media. Journal of Hydraulic Division ASCE 1964;90:1–2.
[46] Hunt ML, Tien CL. Non-darcian convection in cylindrical beds. Journal of Heat Transfer 1988;110:378–84.
[47] Vafai K, Sozen M. Analysis of energy and momentum transport for fluid flow through a porous bed. Journal of Heat Transfer 1990;112:690–9.
[48] VDI. VDI—Wärmeatlas. Dusseldorf: VDI-Verlag, 1997.
[49] Touloukian YS, Buyco EH. Thermophysical properties of matter. New York: IFI/Plenum, 1970.
[50] Vereinigte Thüringische Schiefergruben GmbH & Co. KG, Ortsstr. 44, 7330 Unterloquitz, Germany, 1998.
[51] Schröder E., Bestimmung des Druckverlusts und des Wärmeübergangs von gasdurchströmten Feststoffschüttungen in der PANTHA-Anlage. Technical report, Forschungszentrum Karlsruhe, FZKA 6373, 1999.
[52] Achenbach E. Heat transfer and pressure drop of pebble beds up to high reynolds number. Proceedings of the Seventh International Heat Transfer Conference, 1982. p. S3–8.
[53] Inaba H, Fukuda T. Transient heat transfer behaviours in cylindrical porous beds at relatively large reynolds numbers. Wärme-und Stoffübertragung 1984;18:109–16.
[54] Satterfield CN, Resnick H. Simultaneous heat and mass transfer in a diffusion-controlled chemical reaction. Chemical Engineering Progress 1954;50(10):504–10.
[55] Kung H. A mathematical model of wood pyrolysis. Combustion and Flame 1972;185–195.
[56] Peters B, Gosman AD. Numerical simulation of unsteady flow in engine intake manifolds. In: SAE-Congress 1993, Detroit, SAE-paper 930609, 1993.
[57] Peters B, Bruch C. Evaluation of ODE-solvers for the prediction of thermal conversion of solid fuels. In: Proceedings of the 16th IMACS WORLD CONGRESS 2000, Lausanne, August 21–25, 2000.
[58] Milde M. ODE++ a class library for ordinary differential equations. Technical report, Friedrich-Schiller-Universität Jena, Institut für Angewandte Mathematik, Ernst-Abbe-Platz 1–4, 7740 Jena, 1998.
[59] Milde M. ODE++ a class library for ordinary differential equations. Friedrich-Schiller-Universität Jena, Institut für Angewandte Mathematik, Ernst-Abbe-Platz 1–4, 7740 Jena, 1998.